

Lithospheric rheology and flexure at Artemis Chasma, Venus

C. David Brown and Robert E. Grimm

Department of Geology, Arizona State University, Tempe

Abstract. Artemis Chasma is an arcuate, 2000-km-diameter zone of convergence and lithospheric underthrusting on Venus. Inelastic flexure modeling of the topography at Artemis, combined with observations of trench tectonics, allow us to document local temperature gradients below 4 K km^{-1} and an immense compressive in-plane force at the trench. Lithospheric rheology on Venus may be stronger than would be predicted from conventional extrapolations of rock mechanics experiments; in particular, the brittle surface strength must reach a few tens of megapascals to satisfy the observed lack of flexurally induced surface faulting. Elastic plate bending models provide an adequate estimate of the bending moment at Artemis, but they fail to constrain—or even recognize—the in-plane force. The inelastic analysis implies an in-plane force of the order of $-1 \times 10^{14} \text{ N m}^{-1}$; a potential driving force is thermal thinning of regionally thick lithosphere in the highlands to the north. The low heat flux at Artemis, which is a comparatively young structure, is compatible with the notion that Venus has experienced a prolonged period of cooling in the last several hundred million years. The inference of such exceptionally low thermal gradients embraces three end-member possibilities: (1) the surface age is $>600 \text{ Ma}$, (2) the lithospheric thermal age is greater than the surface age, and/or (3) the upper mantle temperature is anomalously low ($\sim 1550 \text{ K}$).

Introduction

Artemis Chasma is a 2000-km-diameter arcuate trough in Aphrodite Terra, Venus, that is the manifestation of lithospheric underthrusting and intense surface deformation (Figure 1). Our examination of the tectonics of Artemis [Brown and Grimm, 1995] has revealed a coherent, plate-like motion of the circular interior platform which produced southeast vergent deformation on the southeast chasma margin akin to that at terrestrial subduction zones and prominent left-lateral strike-slip displacements on the east margin. Two independent measurements of strain agree that horizontal motions were limited to no more than $\sim 250 \text{ km}$. Artemis is relatively young, both with respect to nearby Aphrodite chasmata as well as in the global stratigraphy, and its tectonics are not directly attributable to mantle plume processes.

Southeast Artemis Chasma is distinguished by its paired ~ 1 -km-deep trench and ~ 1 -km-high outer rise, which Sandwell and Schubert [1992a] interpreted to be analogous to the flexural trench-outer rise structures of subduction zones on Earth. There are several observations in support of a flexural origin for this topography: (1) the tectonic environment is one of lithospheric underthrusting [Brown and Grimm, 1995], which is amenable to flexure caused by surface, subsurface, and horizontal loading; (2) the outer rise is smooth and largely undeformed, indicating it was uplifted not by folding or faulting but by bending of the lithosphere; (3) a gravity high northwest of the trench closely matches the region of geologically inferred convergence, is indicative of the mass anomaly expected from underthrusting [Schubert et al., 1994], and is associated with the loading responsible for the flexure. One observation in

striking conflict with the flexural interpretation is the complete absence of trench-parallel normal faulting on the outer trench wall (Figure 1, inset), a characteristic property of the convex upward bending of the lithosphere at subduction zones [e.g., Jones et al., 1979].

Artemis Chasma is an excellent site for examining flexure on Venus because the lithospheric strength of the underthrust plains should provide a sense of how low the venusian heat flux might be. Other flexure studies have relied on topography and gravity at coronae and volcanoes [Sandwell and Schubert, 1992a; Johnson and Sandwell, 1994; Phillips, 1994; McGovern et al., 1995], which are products of mantle upwelling and magmatism. Sites of lithospheric underthrusting and orogeny, on the other hand, are regions less “contaminated” by thermal anomalies, and they potentially provide more representative constraints on the geotherm of ancient lithosphere. Such information is particularly valuable for comparison to interior thermal evolution models [Turcotte, 1993; Arkani-Hamed et al., 1993; Parmentier and Hess, 1992] invoked to explain the apparently near-uniform surface age of $\sim 400 \text{ Ma}$ [Phillips et al., 1992; Schaber et al., 1992]. Artemis is unique for another reason: its flexural outer rise towers above those of subduction zones on Earth, where outer rises are typically only a few hundred meters high. Conventional flexure models may be inadequate for explaining such topography.

Artemis Chasma Topography

A map view of the topography at the southeast margin of Artemis is provided in Figure 1. The tectonics and structural geology of Artemis as a whole imply northwest-southeast-directed convergence at this boundary, at an azimuth of $\sim 125^\circ$ [Brown and Grimm, 1995]. Sandwell and Schubert [1992a] performed flexural fits to topography on the southern margin where the trench and outer rise may also originate from

Copyright 1996 by the American Geophysical Union.

Paper number 96JE00834.
0148-0227/96/96JE-00834\$09.00

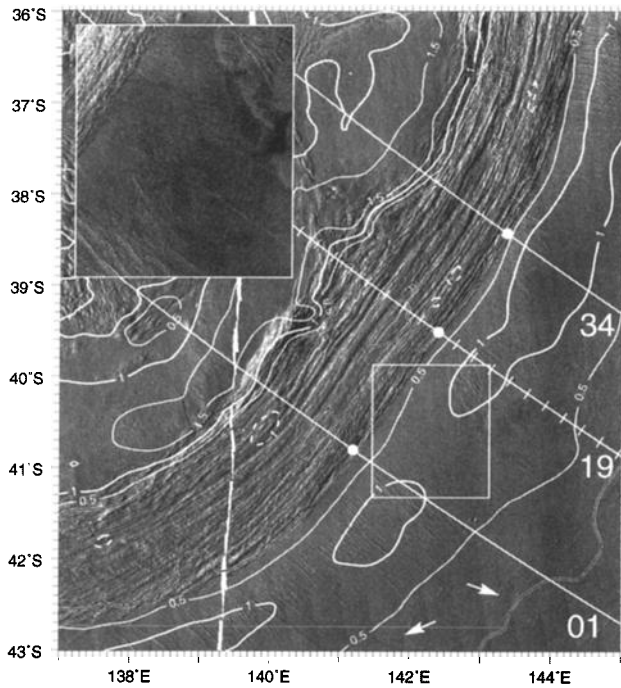


Figure 1. Shaded relief image of the southeast margin of Artemis Chasma. The image, approximately 650 km across, is in equidistant cylindrical projection. Topography is low-pass filtered and contoured in kilometers above mean planetary radius (6051.85 km), which is marked by the unlabeled, striped contour. The three profiles indicated are shown in Figure 7. The arrows point out wrinkle ridges. Profile 19 is marked in 25-km intervals; the dot on each profile denotes the origin. The inset image (left-looking synthetic aperture radar) illustrates the lack of trench-parallel deformation on the outer rise. This image is an enlargement of the boxed area and is 130 km across.

bending, but the loading configuration is probably more complex there.

We define the deformation front of the outer trench slope fold-and-thrust belt as the horizontal origin for our topographic profiles. This nearly linear, ~300-km-long boundary between the severely deformed trench and the smooth, undisrupted plains trends at azimuth 35°; great circle topographic profiles are extracted perpendicular to this feature. We obtain 34 profiles, spaced ~9 km apart (at the trench), by bilinearly interpolating elevations from the Global Topography Data Record (GTDR) [Ford and Pettengill, 1992]. We have examined both the Altimeter-Radiometer Composite Data Record (ARCDR) footprints and the altimeter profiles at the outer rise, and are confident our interpolated profiles accurately represent the topography. The GTDR error data over this region indicate that typical errors are ~50 m, with some orbits peaking at about 100 m.

We characterize the flexural topography at Artemis in two ways. We build an average profile from the 34 original interpolated profiles; this step serves to eliminate some of the short-wavelength noise in the data that is not associated with lithospheric flexure, and it provides us with a representative cross section. Also, for each of the 34 profiles we determine the topographic slope of the plains, the outer rise amplitude and width, and the trench depth. Slopes are small (~0.01°) and

dip to the southeast; they increase in magnitude from southwest to northeast (Figure 2a). The slope is subtracted from each profile before measuring the maximum outer rise amplitude, full width at half-maximum (FWHM) of the outer rise, and maximum trench depth. The amplitude varies from 1160 to 1570 km, generally decreasing from southwest to northeast (Figure 2b). The mean and standard deviation of the amplitude are 1290 ± 90 m. The width ranges from 130 to 255 km, and also decreases from southwest to northeast (Figure 2c). The mean FWHM is 190 ± 35 km. The trench depth shows no consistent trend along strike (Figure 2d). It varies from 450 to 2030 m, with a mean value of 1180 ± 420 m.

Lithospheric Rheology

We employ yield stress envelopes, which define the strength of the lithosphere as a function of depth, in our flexure models [Goetze and Evans, 1979; Kohlstedt et al., 1995]. Yield envelopes represent the maximum stress the lithosphere can sustain at a given depth, and they almost certainly overestimate the net strength [Kirby, 1983; Kohlstedt et al., 1995]. In this section we describe our two assumed rheologic models for the venusian lithosphere. In the “weak” model we follow conventional precepts in designing yield envelopes; these results are therefore most appropriate for comparison to the findings of previous workers. With the “strong” model our approach is to maximize the yield stresses, thereby placing an upper bound on the temperature gradient inferred from flexure modeling. General physical constants are defined in Table 1; the weak and strong rheology model parameters are listed in Table 2.

Brittle Regime

Yield envelopes usually describe the brittle, pressure-dependent strength of the lithosphere with the empirical “Byerlee’s rule” for frictional sliding [Byerlee, 1978], in which strength is a linear function of confining pressure and vanishes at the surface [Brace and Kohlstedt, 1980] (Figure 3).

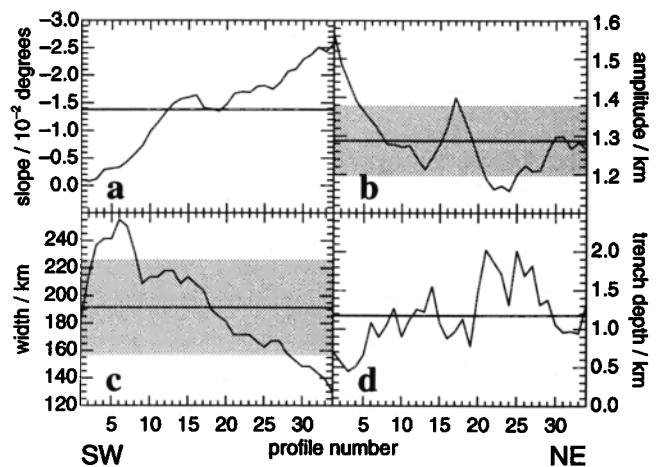


Figure 2. Topographic trends along strike of Artemis Chasma. (a) Topographic slope of plains southeast of Artemis; negative values indicate southeast dips. (b) Outer rise amplitude. (c) Outer rise width at half-maximum amplitude. (d) Maximum trench depth. Horizontal lines signify the mean values; one standard deviation is depicted by shaded regions.

Table 1. Model Parameter Values

Symbol	Definition	Value
A	flow law coefficient	$10^{4.46} \text{ MPa}^{-n} \text{ s}^{-1}$
E	Young's modulus	$6.5 \times 10^{10} \text{ Pa}$
g	gravity at surface	8.87 m s^{-2}
n	flow law stress exponent	3.6
R	molar gas constant	$8.314 \text{ J mol}^{-1} \text{ K}^{-1}$
T_s	surface temperature	740 K
$\dot{\epsilon}_{xx}$	strain rate	10^{-14} s^{-1}
κ	thermal diffusivity	$10^{-6} \text{ m}^2 \text{ s}^{-1}$
ρ_c	crust density	2900 kg m^{-3}
ρ_m	mantle density	3300 kg m^{-3}
ν	Poisson's ratio	0.25

We incorporate Byerlee's rule in the weak rheology model. Application of Byerlee's rule assumes that preexisting faults at suitable orientations are present to accommodate bending strains. If faults of optimum orientation are not available, the brittle strength will be greater, possibly reaching the ultimate fracture strength of the rock [Sibson, 1985].

The lithosphere being flexed at Artemis Chasma may not possess preexisting faults which could accommodate flexure: the surface is smooth and largely undeformed on the plains to the southeast of the trench (Figure 1, inset). Therefore, we are unwilling to assume that Byerlee's rule provides a conservative bound on lithospheric strength. We instead describe the brittle strength in the strong rheology model using a Mohr-Coulomb failure law, which has the form

$$\tau = \tau_0 + (\tan\phi)\sigma_n \tag{1}$$

where τ and σ_n are the shear and normal stresses, τ_0 represents the cohesion, and ϕ is the angle of internal friction. We convert (1) into a form appropriate for constructing yield envelopes by deriving the differential stress $\Delta\sigma = \sigma_1 - \sigma_3$ [e.g., Jaeger and Cook, 1969, pp. 87–91] for compression and tension, where σ_3 and σ_1 , respectively, equal the confining pressure ($\rho_m g z$).

We assume that $\tan\phi$ in (1) is equal to the coefficient of sliding friction; following Byerlee [1978], we assign $\tan\phi = 0.85$ for $\sigma_n \leq 200 \text{ MPa}$ and $\tan\phi = 0.60$ for $\sigma_n \geq 200 \text{ MPa}$. The compressive fracture strength has values of $\sim 150\text{--}400 \text{ MPa}$ for common mafic rocks (basalt, diabase, gabbro, and dunite) [Shimada et al., 1983; Goodman, 1989, p. 61]. Equivalent cohesion values are $\sim 35\text{--}90 \text{ MPa}$. We let $\tau_0 = 50 \text{ MPa}$ in the strong model. The Mohr-Coulomb model overestimates the strength of the upper lithosphere because experiments indicate brittle fracture strength increases nonlinearly with increasing confining pressure [e.g., Paterson, 1978, pp. 21–28]. A

Table 2. Lithospheric Rheology Models

Symbol	Definition	Weak	Strong
τ_0	cohesion, MPa	0	50
Q	activation energy, kJ mol^{-1}	535	560
V^*	activation volume, $\text{cm}^3 \text{ mol}^{-1}$	0	17

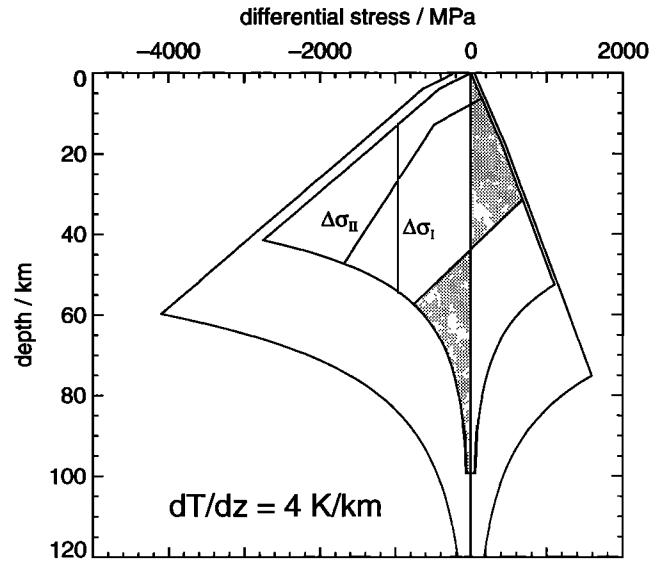


Figure 3. Weak rheology (inner) and strong rheology (outer) yield strength envelopes at 4 K km^{-1} . The stress profile at a bending curvature of $+8 \times 10^{-7} \text{ m}^{-1}$ is indicated by the shaded area. The base of the strong envelope is located at 153 km depth. The stress profile for a compressive in-plane force ($-6 \times 10^{13} \text{ N m}^{-1}$) with no bending ($\Delta\sigma_I$) and following bending to a curvature of $+5 \times 10^{-7} \text{ m}^{-1}$ ($\Delta\sigma_{II}$) are also shown (the kink in $\Delta\sigma_{II}$ reflects elastic unloading).

comparison of the Mohr-Coulomb failure strength to Byerlee's rule is depicted in Figure 3.

Ductile Regime

Laboratory experiments show that rocks experience ductile creep at elevated temperatures. Empirically, stress is seen to be related to strain rate by a power law relationship:

$$\Delta\sigma = \left(\frac{\dot{\epsilon}_{xx}}{A} \right)^{1/n} \exp \left(\frac{Q + V^*P}{nRT} \right) \tag{2}$$

where the coefficient A , stress exponent n , activation energy Q , and activation volume V^* have values determined by laboratory measurements. In Figure 4 we have plotted (2) as a function of temperature for dry diabase [Mackwell et al., 1995] and four different anhydrous olivine and dunite flow laws. The strength of natural polycrystalline dunite [Chopra and Paterson, 1984], synthetic olivine aggregates [Karato et al., 1986], and Goetze's [1978] high-temperature olivine are very similar. Clearly, diabase is weaker at all temperatures. An upper limit on the strength of olivine is provided by the strongest slip system, (010)[001]; the constitutive equation for this system, determined by Bai et al. [1991], is also plotted in Figure 4.

How certain are we that these flow laws represent the maximum yield stresses that can be sustained by the venusian lithosphere? Mackwell et al. [1995] demonstrated the dramatic increase in the strength of diabase produced by ensuring samples were properly dehydrated. Chopra and Paterson [1984] were even more thorough in drying their samples, and they measured the water content using infrared spectroscopy, finding little change in strength below 0.01 weight percent H_2O . The agreement between the three anhydrous polycrystalline

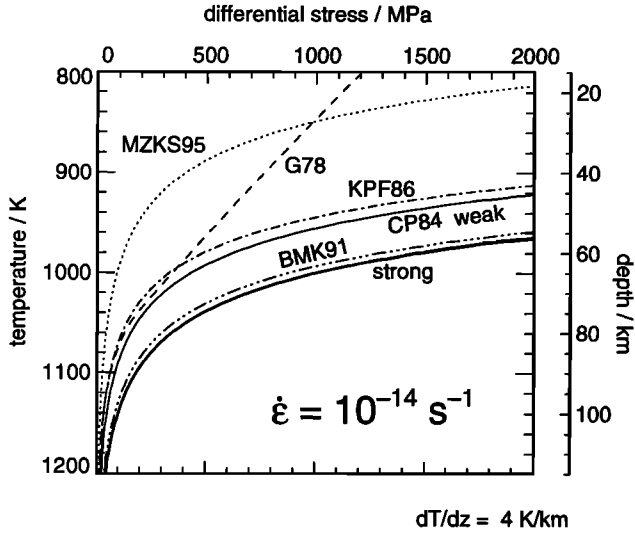


Figure 4. Differential stress as a function of temperature for several anhydrous rock flow laws; a depth scale is also provided for 4 K km⁻¹. MZKS95: Columbia diabase (Ni–NiO buffer) [Mackwell *et al.*, 1995]. G78: Goetze [1978] olivine flow laws; the nearly linear segment is a low-temperature Dorn law. KPF86: Karato *et al.* [1986] synthetic olivine aggregate power law. CP84: Chopra and Paterson [1984] polycrystalline dunite power law, the weak ductile rheology used in this study. BMK91: (010)[001] slip system constitutive equation for olivine single crystals (opx buffer, IW oxygen fugacity [Myers and Eugster, 1983]) [Bai *et al.*, 1991]. The strong ductile rheology used in this study is plotted with the bold, solid line.

dunite flow laws (Figure 4) is reassuring, and we doubt that laboratory experiments will find dunite to be significantly stronger.

Also of possible concern is the need to extrapolate from experimental temperatures of ~1500–1800 K to mechanical lithosphere conditions of <1100 K. Experimental results suggest that, to a very good approximation, the activation energy for dislocation creep is independent of temperature over the tested range. At lower temperatures (and higher stresses) the power law behavior of crystal creep breaks down, and distinct, weaker processes dominate [Kirby, 1983; Tsenn and Carter, 1987]. Evans and Goetze's [1979] olivine hardness tests over a broad temperature range (300–1800 K) revealed a sharp decrease in strength at reduced temperatures. They suggested that a Dorn law, in which creep rate depends exponentially on stress, applies at $\Delta\sigma > 200$ MPa [Goetze, 1978] (Figure 4). Therefore, power laws overestimate lithospheric strength.

In the weak rheology model we let the ductile strength of the mantle be described by Chopra and Paterson's [1984] flow law (Figure 4). For the strong rheology model we assume that Bai *et al.*'s [1991] (010)[001] slip system constitutive equation places an upper bound on the strength of the venusian mantle. For convenience, we retain Chopra and Paterson's [1984] values of A and n , and simply raise the activation energy to 560 kJ mol⁻¹ (Figure 4). We also include an activation volume [Kirby, 1983]. In both rheology models, ductile stresses are calculated at a strain rate of 10⁻¹⁴ s⁻¹, a reasonable upper bound for a convergent setting, and the base of the mechanical lithosphere ($z = h_m$) is defined by a ductile strength of 50 MPa.

In our flexure modeling we ignore the role of the crust in the lithospheric strength. The crust of the venusian plains is ~20–50 km thick [Grimm and Hess, 1996], and the lower crust might experience ductile flow. However, at Artemis the crust has not become decoupled from the upper mantle lithosphere despite the intense underthrusting, implying that the crust and mantle are mechanically welded [Brown and Grimm, 1995]. By neglecting the crust we adhere to our principle of maximizing the inferred thermal gradients.

Elastic Plate Bending Analysis

To allow us to compare our results to those of Sandwell and Schubert [1992a], and to form a basis of comparison for our inelastic flexure models which follow, we fit an analytic elastic plate bending equation to the Artemis Chasma topography. We consider a very general elastic solution for the vertical displacement (w) as a function of distance (x) [Parsons and Molnar, 1976]:

$$w(x) = \left[-\frac{2\alpha\beta}{N_{cr}} \left(M + \frac{Nw_0}{2} \right) \sin\left(\frac{x}{\beta\lambda}\right) + w_0 \cos\left(\frac{x}{\beta\lambda}\right) \right] \times \exp\left(-\frac{x}{\alpha\lambda}\right) + mx + z_0 \quad (3)$$

$$\alpha = \left(1 - \frac{N}{N_{cr}} \right)^{-1/2} \quad (4a)$$

$$\beta = \left(1 + \frac{N}{N_{cr}} \right)^{-1/2} \quad (4b)$$

Note that w is defined positive down. $N_{cr} = -4D\lambda^2$ is the compressive buckling in-plane force, where the flexural wavelength is defined as

$$\lambda = \left(\frac{4D}{\Delta\rho g} \right)^{1/4} \quad (5)$$

and the flexural rigidity is a function of the elastic plate thickness (h_e)

$$D = \frac{Eh_e^3}{12(1-\nu^2)} \quad (6)$$

The mantle-surface density contrast is $\Delta\rho = \rho_m$. We initially let the in-plane force per unit length (N) be zero, and perform a nonlinear least squares fit [Press *et al.*, 1992, pp. 683–688] of (3) to a ~1500-km length of the average profile with five free parameters: the bending moment per unit length (M) applied at the trench, the trench depth (w_0), the topographic slope (m), the vertical offset (z_0), and the flexural wavelength (λ). Other parameters and their values are specified in Table 1. The plate curvature is defined as $K = d^2w/dx^2$, and the elastic bending moment is given by $M = -DK$.

The application of the elastic analysis to the average profile yields $h_e = 56$ km, over 20% greater than Sandwell and Schubert's [1992a] result for the southern chasma; the fit is shown in Figure 5. We have not directly estimated the uncertainty of h_e , but it realistically is at least 10 km [McQueen and Lambeck, 1989]. The maximum curvature and bending moment (which are probably even more poorly determined) are 7.8×10^{-7} m⁻¹ and -7.9×10^{17} N, respectively.

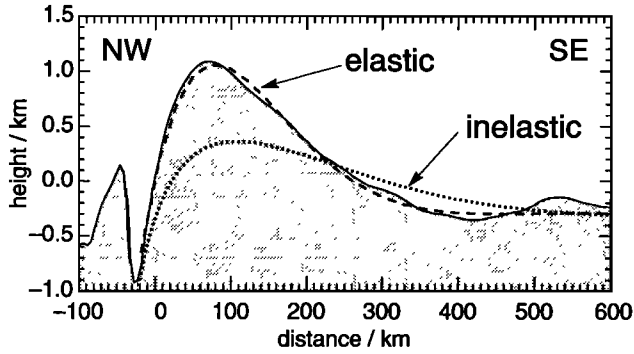


Figure 5. Average topographic profile, vertically exaggerated by a factor of 145. Elastic plate bending model fit (dashed) and inelastic flexure model fit (dotted) are plotted. The inelastic profile was created at the 4 K km^{-1} geotherm calculated by matching the first zero crossing moment–curvature pair of the elastic solution to identical values for an inelastic rheology; the applied bending moment is $-6.8 \times 10^{17} \text{ N}$, and the trench depth boundary condition is 1.1 km. No in-plane force is included.

To estimate the mechanical plate thickness (h_m) and linear temperature gradient (dT/dz) that relate to the elastic model, we apply the moment–curvature matching technique of *McNutt and Menard* [1982]. We assume the moment and curvature of the elastic model at the first zero crossing equal the M – K pair for an inelastic lithosphere in which stresses are limited by the yield envelope. We iteratively calculate the inelastic moment at the elastic curvature as a function of thermal gradient (with the weak rheology), and find agreement with the elastic moment at $dT/dz = 4.0 \text{ K km}^{-1}$, which corresponds to $h_m = 99 \text{ km}$. This geotherm is similar to that determined by *Sandwell and Schubert* [1992a].

Inelastic Flexure Modeling

Model Theory and Solution

The solution to the inelastic bending of the lithosphere must satisfy the force balance for the large deflection and finite deformation of a plate [*Fung*, 1965, pp. 463–470; *Liu*, 1980; *Mueller and Phillips*, 1995]:

$$\frac{d^2 M(x)}{dx^2} = - \left[\frac{dN(x)}{dx} + \sigma_{xz}(x, h_m) \right] \frac{dw(x)}{dx} - N(x) \frac{d^2 w(x)}{dx^2} + \Delta \rho g w(x) \quad (7)$$

where $\sigma_{xz}(x, h_m)$ is a basal shear traction. Equation (3) is an analytic solution to (7) for a purely elastic plate (with σ_{xz} equal to zero), but for our inelastic modeling we require numerical solutions. A condition of (7) is that the horizontal strain and bending slope (dw/dx) are small compared to unity. Both parameters are $<5\%$ at Artemis based on the slopes and curvatures in the elastic fit.

To reduce (7) to a single independent variable (w), we must construct a relationship between curvature and bending moment [*Mueller and Phillips*, 1995]. For each curvature we determine a stress profile subject to the plastic strength limits of the yield envelope, assuming a Tresca yield criterion. Elastic core stresses are related to the curvature by

$$\Delta \sigma(z) = - \frac{E(z - z_n) K}{(1 - \nu^2)} \quad (8)$$

where z_n is the neutral surface depth, which is iteratively determined by the requirement that the horizontal stress resultant equal the in-plane force:

$$N = \int_0^{h_m} \Delta \sigma(z) dz \quad (9)$$

Having determined the full stress profile, we can proceed to calculate the bending moment:

$$M = \int_0^{h_m} \Delta \sigma_{II}(z) z dz - \int_0^{h_m} \Delta \sigma_I(z) z dz \quad (10)$$

Here the bending moment is represented by the difference in moment of the net stress distribution of the in-plane force and bending ($\Delta \sigma_{II}(z) \Delta \sigma(z)$ of (9)) and the in-plane stress distribution at zero curvature ($\Delta \sigma_I(z)$) (Figure 3). Our model assumes that the in-plane force is applied prior to bending, and it accounts for the effects of elastic unloading following plastic failure [*McAdoo et al.*, 1978; *Mueller et al.*, 1996].

By reducing (7) to four first-order differential equations and employing the moment–curvature relationship, we solve the flexure equation as a two-point boundary value problem using a finite difference routine [*Phillips*, 1990; *Mueller and Phillips*, 1995]. We specify the displacement and applied moment on the left (trench) end of the profile; the boundary conditions on the right end are zero displacement and curvature. We initially neglect σ_{xz} and assume N is constant with distance.

Evaluation of Elastic Model Results

Figure 5 includes an inelastic flexure curve for the same temperature gradient implied by the elastic modeling: 4 K km^{-1} (weak rheology). Clearly, this solution fails, as the outer rise amplitude is just half the observed height. Perhaps this shortcoming can be explained by a failure of the first zero crossing moment–curvature matching technique [*McNutt and Menard*, 1982]. *Mueller and Phillips* [1995] showed that this method systematically underestimates h_m but using the maximum moment–curvature values instead results in a far more accurate determination. In this case, the latter method yields $dT/dz = 3.6 \text{ K km}^{-1}$ ($h_m = 111 \text{ km}$), only a minor change, and yet there is no improvement to the modeled fit.

From the inelastic modeling perspective a given geotherm and strength envelope will limit the maximum bending moment (and outer rise height) allowed. For instance, the saturation moment at 3.6 K km^{-1} is $-8.8 \times 10^{17} \text{ N}$, so very little additional amplitude can be attained in the inelastic model by increasing the applied moment. A higher geotherm would further limit the maximum attainable flexural amplitude, whereas a lower geotherm would produce an inappropriately long flexural wavelength. Therefore, unlike elastic plates, an arbitrarily large outer rise height cannot be generated by an inelastic lithosphere for all flexural wavelengths. Recognizing this additional constraint, is it possible to explain the Artemis outer rise in the context of an inelastic, finite-strength lithosphere?

The inclusion of an in-plane force introduces an additional modeling parameter. It, too, is limited by the net strength of the lithosphere (i.e., (9) with $\Delta \sigma(z)$ equal to the compressional or tensional yield strength), but it modulates both the flexural amplitude and wavelength. The latter property can be seen in

(3) and (4) for the elastic plate: the sinusoidal wavelength ($\beta\lambda$) is decreased by a compressive in-plane force, and the damping wavelength ($\alpha\lambda$) is increased. Similar behavior occurs with inelastic plate flexure. This insight suggests that an in-plane force may play a crucial role in the Artemis Chasma topography, and it might explain the failure of the inelastic model depicted in Figure 5.

We have attempted to obtain least squares fits of equation (3) to the Artemis trench–outer rise with N as a sixth free parameter. However, the in-plane force is completely undetermined: varying N by up to 10^{14} N m $^{-1}$ in both compression and tension fails to improve the rms error at any value. This finding verifies the more complete analysis of *Mueller and Phillips* [1995]. In all fits the values of h_e are similar to the $N = 0$ results. We therefore proceed with our fully inelastic modeling.

Inelastic Model Results

Our approach is to explore the three-dimensional parameter space of temperature gradient, in-plane force, and applied bending moment (with an additional degree of freedom provided by the rheological models) by forward modeling with inelastic flexure solutions. Our goal is to match the observed outer rise height and FWHM of Artemis. The results are not sensitive to the trench depth boundary condition, which we set to 1 km (Figure 2d). An example of the output of our model is depicted in Figure 6. This interaction diagram delineates the saturation moment (for positive curvatures) as a function of in-plane force for a thermal gradient of 5 K km $^{-1}$ and the strong rheology. The saturation moment is the maximum bending

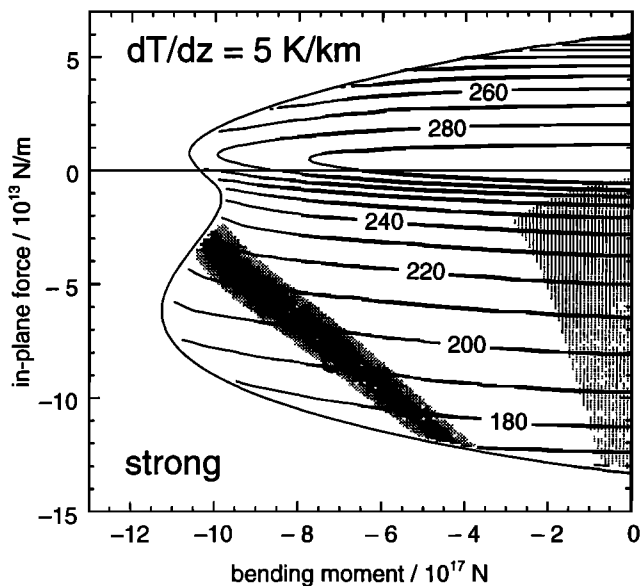


Figure 6. In-plane force–bending moment interaction diagram for the strong rheology at 5 K km $^{-1}$. The sinuous envelope corresponds to the saturation moment as a function of in-plane force. Outer rise width from inelastic model solutions is contoured in kilometers. The diagonal shaded band marks agreement with both the observed outer rise amplitude and width to within two standard deviations. The stippled area at right indicates conditions at which no surface failure occurred. Circle corresponds to Figure 7a.

moment that an elastic–plastic lithosphere can sustain, and it is reached as curvature increases. Bending on the outer trench walls of convergent zones is characterized by positive curvatures, and we do not pursue solutions with negative curvatures at this boundary. Large positive applied moments would result in an upturn in the deflection profile at the intended trench.

Within the diagram (Figure 6) we have contoured the FWHM of the modeled outer rise as a function of in-plane force and bending moment at the trench. The outer rise width is a maximum at $N = 0$, and it decreases with both tensional and compressional in-plane forces. This behavior parallels that of the elastic plate (equation (3)), but it can also be viewed as a consequence of the thinning elastic core when an in-plane force is applied (Figure 3). Figure 6 and corresponding diagrams for other geotherms demonstrate that the FWHM is primarily a function of the in-plane force and the mechanical plate thickness; therefore, the observed outer rise width alone should provide constraints on the allowed combinations of N and dT/dz .

The oblique shaded band in Figure 6 marks the inelastic flexure model solutions that satisfy both the mean amplitude and FWHM of the Artemis outer rise to within two standard deviations. The amplitude is dependent on both the in-plane force and applied moment, as we would expect from the elastic solution (equation (3)). These results imply that the in-plane force must be compressional and quite large—no zero in-plane force solutions are capable of reproducing the ~ 1.3 -km outer rise height. Inferred applied bending moments, too, are very large. The results shown in Figure 6 are not unique, and they do not explain the entire observed range of the FWHM (Figure 2c). We must invoke higher and lower thermal gradients to produce narrower and wider outer rises, respectively, for this rheology. However, the along-strike variation in the FWHM could also be explained by a constant geotherm but a nonuniform rheology (e.g., a changing crustal thickness). Similar diagrams built at other geotherms and using the weak rheology mirror the patterns seen in Figure 6; in particular, a compressional in-plane force is always required.

Figure 6 illustrates our ability to satisfy the amplitude and width of the Artemis outer rise with the inelastic flexure model, but convincing solutions must also match the slopes of the outer rise flanks. In Figure 7 we demonstrate that complete inelastic model solutions provide good fits to typical topographic profiles of the southeast chasma for the parameter values indicated by plots such as Figure 6. In some cases there are disparities on the outer trench wall, but we emphasize that these solutions are not unique; other combinations of dT/dz , N , and M can provide equivalent or better fits. Typical rms misfits are ~ 100 – 150 m.

To determine if a basal shear traction might affect the magnitude of the loads, we have also solved (7) for nonzero, constant σ_{xz} (in which the in-plane force is a linear function of x). Because of the x dependence of N , we must create a moment–curvature–in-plane force surface to solve (7); we bilinearly interpolate over this surface to determine the curvature at a given N and M . We find that these inelastic profiles are essentially indistinguishable from those with constant N and zero σ_{xz} when the distance over which N varies is long (~ 1000 km). The outer rise shape is slightly altered by the decrease in N with distance from the trench, but the basal shear stress apparently does not modify the flexural signature because it is of the order of 10 times less than the bending stresses.

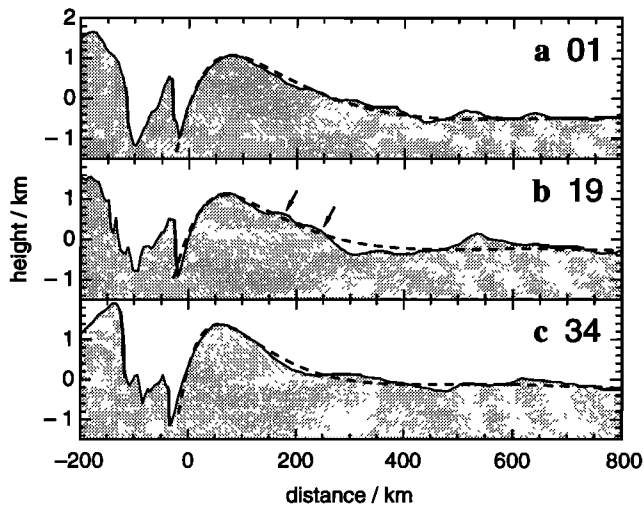


Figure 7. Inelastic model fits to three topographic profiles indicated in Figure 1, vertically exaggerated by a factor of 73. (a) Strong rheology, $dT/dz = 5 \text{ K km}^{-1}$, $N = -8.5 \times 10^{13} \text{ N m}^{-1}$, $M = -7.2 \times 10^{17} \text{ N}$. (b) This profile is similar in shape to the average profile (Figure 5). Weak rheology, $dT/dz = 3.6 \text{ K km}^{-1}$, $N = -1.0 \times 10^{14} \text{ N m}^{-1}$, $M = -3.5 \times 10^{17} \text{ N}$. The arrows mark a ridge that may be unrelated to the flexural topography, and which therefore exaggerates the outer rise width. (c) Strong rheology, $dT/dz = 7.3 \text{ K km}^{-1}$, $N = -4.1 \times 10^{13} \text{ N m}^{-1}$, $M = -3.6 \times 10^{17} \text{ N}$.

Absence of Surface Faulting

Another feature of Figure 6 is the domain in which no surface failure occurs, marked by the stippled area. Surface normal faulting is induced when bending curvatures are large enough for the stress profile to intersect the Mohr-Coulomb envelope in tension (Figure 3); thus, the zone of no failure is confined to relatively small moments. The surface is always at failure in the weak rheology model because the surface strength is assumed to be zero. There is an enormous discrepancy between the inferred in-plane force and applied moment (constrained by the outer rise amplitude and FWHM) and the conditions of no surface failure (Figure 6). The bending curvatures at Artemis are so large ($\sim 7\text{--}10 \times 10^7 \text{ m}^{-1}$) that it appears to be impossible to avoid surface failure, a situation that persists at other thermal gradients.

A very simple way in which to prevent surface faulting is to assume a higher brittle strength; however, for most parameter combinations a cohesion of at least 200 MPa is necessary. The widespread deformation on Venus indicates that the strength of surface materials is probably not this large; such a cohesion is also contrary to most laboratory measurements of the fracture strength of rocks [Schultz, 1993].

So far we have assumed a very simple loading sequence: an in-plane force is applied first, perhaps associated with a regional stress in the downgoing lithosphere, and bending follows as the lithosphere is distorted at the outer rise. Therefore, at shallow depths, the lithosphere first fails in compression because of the in-plane force; with bending, elastic unloading occurs until the tensional yield strength is reached [Mueller *et al.*, 1996] (Figure 8). This is the cause of the dominant surface failure in the flexure models: elastic unloading does not progress far before tensional failure is reached despite the compressional in-plane force.

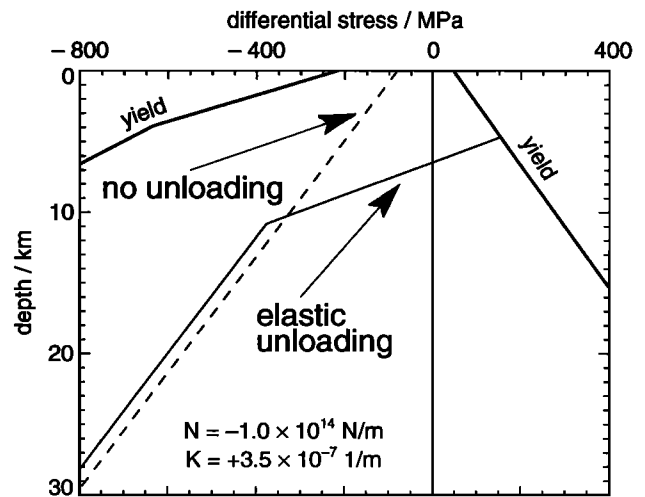


Figure 8. Comparison of lithospheric stress distributions with (solid) and without (dashed) elastic unloading; brittle strength envelope is marked by bold lines. In the former case, the in-plane force was completely applied prior to any bending; depths initially in compressive plastic failure yield in tension at even moderate bending curvatures. If the application of the in-plane force and the occurrence of bending are synchronous, near-surface failure is precluded because the lithosphere never fails in compression (“no unloading”).

A possible means to avert unloading is for the in-plane force magnitude to track the bending curvature such that the surface stress never intersects the yield envelope on the outer rise. With time, a given point on the surface could experience both a gradually increasing compressional in-plane force and bending such that the surface stress remains approximately zero. Because the curvature increases almost linearly from the back flank of the outer rise to the trench, surface faulting would be precluded if the in-plane force increases in a similar manner toward the trench.

The spatial arrangement of wrinkle ridges on the plains southeast of Artemis is suggestive of the variation in surface stress (Figure 1). The wrinkle ridges, which reflect shortening, trend roughly parallel to the chasma, and they extend for thousands of kilometers across the plains. However, the wrinkle ridges are conspicuously absent on the outer trench wall and outer rise peak—thus, there is neither extensional nor contractional deformation in this zone. The position where the wrinkle ridges end on the back side of the outer rise is near where the flexural models predict a change in sign of the curvature. Therefore, the wrinkle ridges are another manifestation of the compressive in-plane force, and their formation has been inhibited on the outer rise because bending stresses canceled the in-plane stresses.

We can simulate the proposed relationship between in-plane force and bending in our models by leaving out elastic unloading when constructing the stress profiles (Figure 8); we thereby assume no initial compressional failure has occurred. With this modification we discover that we can now find conditions that satisfy all three key observables at Artemis: the outer rise width and height and the lack of surface deformation (Figure 9). This model is an approximation because we have not included the postulated lateral in-plane force variation in

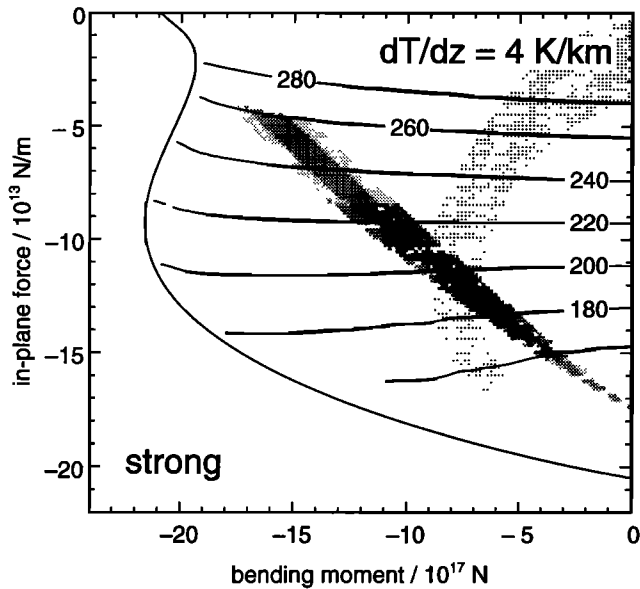


Figure 9. Interaction diagram for inelastic flexure in which the in-plane force and bending are applied concurrently. Strong rheology is illustrated at 4 K km^{-1} . Notice that surface failure can be averted at the large bending moments required to reproduce the Artemis Chasma outer rise amplitude and width (compare Figure 6).

the flexural solutions. For a typical profile (Figure 7a) the constant in-plane force model indicates a need for a factor of 2 or 3 change in N across the outer rise to avoid surface failure with the implied change in curvature. Our model that allows a laterally variable in-plane force indicates that such a change over only 100–200 km will appreciably decrease the outer rise height, implying that still larger forces and moments are required.

Discussion

Our inelastic flexural modeling indicates that the elastic solution coupled with the moment–curvature matching technique succeeds in estimating the approximate geotherm at Artemis, but it fails to distinguish the presence of a large, compressive in-plane force. To understand the seeming contradiction between these two results, we have run accuracy tests for the elastic flexure methods using an approach similar to that of *Mueller and Phillips* [1995]. The elastic plate equation is fit to a series of synthetic inelastic flexure profiles which are generated for different values of in-plane force (N is assumed to be zero in the elastic fits). For each fit we perform the moment–curvature matching calculation for both the first zero crossing and maximum curvatures. We find that the mechanical lithosphere thickness estimated via the elastic fit can be in error by up to $\sim 30\%$ for compressional in-plane forces, depending on such factors as the thermal gradient, trench depth, and applied moment. The errors can be even larger for in-plane tension.

These findings intimate that flexure modeling of terrestrial subduction zones, where stresses ranging from tension to compression can arise from interplate coupling and the transmittal of slab-pull forces [e.g., *Spence*, 1987], might be inaccurate because of the neglect of in-plane forces [*Mueller and*

Phillips, 1995]. For Artemis the agreement between the temperature gradient estimates of the elastic and inelastic solutions is attributed to the range of permissible geotherms with the in-plane force as a free parameter in the inelastic model. For instance, the moment-matching technique predicts a geotherm of 3.3 K km^{-1} for the maximum curvature of an elastic fit to profile 1 (Figure 7a). Inelastic model solutions from 3 to 4 K km^{-1} , a range of 25% in thermal gradient, provide good fits under the weak rheology with variable in-plane force and applied moment.

To place an upper bound on the temperature gradient, we consider the highest geotherm that includes the maximum FWHM within the range of acceptable solutions. However, forward-modeled fits (Figure 7) indicate that the widest outer rise can be satisfactorily fit by somewhat narrower synthetic profiles. In addition, some of the topography on the southeast-facing outer rise slope may not be flexural (arrows, Figure 7b), exaggerating the measured FWHM. We have calibrated this uncertainty by comparing synthetic profiles to the widest portions of the outer rise, and accept 210 km as the maximum FWHM for limiting the geotherm. Taking this adjustment into account, the upper bounds implied by the weak and strong rheology models are 3.4 and 5.1 K km^{-1} , respectively. When the condition of no surface faulting is incorporated into the strong model, the upper bound is 3.8 K km^{-1} ; this value is somewhat less precise because our solutions do not include the spatially variable in-plane force. Narrower segments of the outer rise can be explained by higher thermal gradients or by locally weaker rheology.

A broad range of geotherms, in-plane forces, and applied moments is allowed because of the nonuniqueness of the solutions (Table 3), but these three parameters are strongly interdependent when constrained by the outer rise width and height (Figures 6 and 9). Our inelastic model is relatively sensitive to the $\sim 90\text{-m}$ variations in the amplitude (Figure 2b), which are explained by small changes in the applied loads. The $\sim 35\text{-km}$ variations in the width (Figure 2c) imply changes in some combination of temperature gradient, lithospheric rheology, and in-plane force. Such changes must occur over the trench length of $\sim 300 \text{ km}$ covered by our profiles (Figure 1).

Sources of Loads

In-plane force. A typical compressive in-plane force required by the flexural fits to Artemis is $-1 \times 10^{14} \text{ N m}^{-1}$, although it may be locally lower (Table 3). The observation of a lack of surface faulting near the chasma implies that this

Table 3. Inelastic Flexure Model Results

Parameter	Weak Rheology*	Strong Rheology†
<i>Full Outer Rise Width Range‡</i>		
$dT/dz, \text{ K km}^{-1}$	3.4–5.4	3.8–6.4
<i>Mean Outer Rise Width</i>		
$dT/dz, \text{ K km}^{-1}$	2.8–4.0	3.8–4.4
$N, \text{ N m}^{-1}$	$-(3.0\text{--}15) \times 10^{13}$	$-(9.3\text{--}14) \times 10^{13}$
$M, \text{ N}$	$-(3.5\text{--}15) \times 10^{17}$	$-(4.9\text{--}10) \times 10^{17}$

* Two constraints: outer rise height and width.

† Three constraints: outer rise height and width and no surface failure.

‡ Upper bounds to geotherm over range of outer rise widths.

force decreases from the trench across the outer rise, but it persists for thousands of kilometers into Nsomeka Planitia. The region south of Artemis lacks any candidate features that might provide the requisite driving stresses or the strains accommodating the convergence at Artemis [Brown and Grimm, 1995]. The chasmata and highlands to the north are more plausible source regions. We infer that the in-plane force is transmitted from the overriding plate to the downgoing lithosphere by congested motion at Artemis. The absence of pore fluids on Venus, hence large frictional stresses, is a likely explanation for highly coupled underthrusting compared to terrestrial subduction zones.

A possible cause of the in-plane driving force is mantle flow tractions applied to the base of the lithosphere, aided by the probable lack of a low-viscosity zone on Venus [Phillips, 1986, 1990]. Phillips [1990] derived relationships between in-plane stress and long-wavelength gravity for a thin elastic lithosphere overlying an isoviscous mantle. We have examined the long-wavelength geoid in the Artemis region up to degree 10 (wavelengths ~ 4000 km and greater) using the spherical harmonic gravity model (MGNP90LSAAP [Sjogren et al., 1996]). The theory should be valid at these wavelengths assuming the depth of the density anomaly driving the flow is shallower than ~ 400 km [Phillips, 1990]. The maximum geoid height is ~ 70 m over southeast Thetis Regio, corresponding to a predicted in-plane force of -1×10^{13} N m $^{-1}$, considerably less than the flexurally derived values. However, partial crustal compensation of Thetis [Grimm, 1994] might obscure the presence of a stronger mantle anomaly.

Differential topography is a related mechanism for generating stresses in the lithosphere (e.g., ridge push in oceanic lithosphere). The in-plane force produced by topography is given by the moment of the anomalous density [Dahlen, 1981]. For a very simple configuration of thermally thinned lithosphere the in-plane force is approximately $N = -\rho_m g h L$, where h is the topographic relief and L is the ambient thickness of the thermal lithosphere. For a 4 K km $^{-1}$ geotherm, $L \approx 500$ km for a half-space cooling model. There is roughly 3 km of relief between southeast Artemis and the rifts south of Thetis; thus, $N \approx -4 \times 10^{13}$ N m $^{-1}$. Phillips [1990] pointed out that the geoid expression of topographic stresses [Dahlen, 1981] is identical to his result for flow coupling.

The required driving force per unit length might be less if the area over which it is applied is larger than the ~ 800 -km-long southeast chasma where stresses are presumably focused. The maximum length over which the force could be applied is the diameter of Artemis (2000 km). Therefore, the driving force could be, at most, a factor of 2.5 smaller than the flexurally derived force; that is, it must be at least -4×10^{13} N m $^{-1}$, and it is probably substantially larger. Such enhancement of the driving force makes the mechanisms suggested above marginally acceptable.

The postulated decrease in the in-plane force from the trench to the outer rise connotes that a regional stress has not been continuously applied to the downgoing lithosphere. A regional in-plane force would have produced contractional deformation on the trench slope, either before flexure commenced or before that section of the crust passed through the outer rise. Therefore, the in-plane force and flexure may have grown with time, maintaining the surface stresses near zero.

Bending moment. The large applied bending moments (typically -7×10^{17} N) that we have inferred also present a dilemma: what is their source if the slab beneath Artemis is no

more than ~ 250 km long [Brown and Grimm, 1995]? Terrestrial subduction zones, with much longer slabs, rarely exhibit bending moments greater than -3×10^{17} N [e.g., Levitt and Sandwell, 1995]. The large gravity anomaly at Artemis [Schubert et al., 1994] implies a negatively buoyant slab, and it must contribute to the moment applied at the trench. However, it is unclear how the buoyancy of a slab on Venus would compare to one of similar dimensions on Earth: while the venusian lithosphere may be older than that subducting on Earth, the crust could also be thicker. We might ask whether there is any correlation between such slab characteristics as age, length, and dip and the flexurally derived bending moments for terrestrial subduction zones.

To answer this question, we have calculated the moments (torques) induced at the trench by the negative buoyancy of subducted slabs, using the thermal model of McKenzie [1969] and the parameters of Jarrard [1986], and we compared them to the flexural first zero crossing bending moments reported for 15 subduction zones [McNutt and Menard, 1982; McNutt, 1984; Levitt and Sandwell, 1995]. We find no meaningful correlation between the slab-pull moment and the flexural moment, a result that might be explained by the scatter in reported flexural moments, which can exceed an order of magnitude for a given trench. However, there is also no correlation between the slab moment and maximum flexural moment. This finding can be interpreted as evidence that other factors dominate the relationship between slab thermal buoyancy and flexure at the trench, such as phase changes within the slab, interplate friction, stress transmittal through the mantle wedge, viscous resistance of the mantle, and inhibited penetration of the lower mantle [Davies, 1980, 1981]. It is notable, though, that Jarrard [1986] (using the same thermal model) found a correlation between the predicted slab-pull force and trench depth, another flexural property.

A force not acting at terrestrial subduction zones may contribute to the loading at Artemis. Sandwell and Schubert [1992b] suggested that perhaps topography northwest of the trench loads the underthrust plate. This inner ridge (Figure 1) might be a consequence of the convergence at Artemis, as uplift of the overriding plate has been measured for terrestrial subduction zones. On Earth such topography is rapidly eroded, and it may not play a significant role in the slab force balance. Because our models do not include this region, any vertical loading northwest of the trench is implicitly accounted for in the applied bending moments.

Summary. The fact that the requisite in-plane driving forces are not evident in the gravity field means that the proposed mechanisms are incorrect, the force is not fully expressed in the geoid, or the flexural rise is a relict feature, frozen in by the cooling lithosphere. The dominant source of the applied bending moment is the negatively buoyant slab. The lack of correlation between slab properties and flexural moments at subduction zones affirms that the short Artemis slab is not discrepant with the large moment, as long as the slab-pull torque exceeds the flexural moment. For Artemis the slab must have a shallow dip and a large density anomaly to supply the inferred moment. Paradoxically, given the "missing" in-plane driving force, Artemis should be active or very young, as the slab has not yet thermally assimilated.

Implications for Venus Thermal Evolution

Artemis Chasma, and possibly Latona Corona [Sandwell and Schubert, 1992a], stand alone with exceptionally low heat

flow estimates compared to other features on Venus [Phillips *et al.*, 1996]. Our results imply a thermal gradient no greater than 4 K km^{-1} to explain the maximum outer rise width under the strong rheology with the adjunct condition of no surface faulting. Studies of several coronae indicate geotherms of approximately 6 to 24 K km^{-1} [Sandwell and Schubert, 1992a; Johnson and Sandwell, 1994]. The gravity anomalies over large volcanoes imply thermal gradients of 5 – 7 K km^{-1} [McGovern *et al.*, 1995]; Phillips [1994] estimated a 7 – 10 K km^{-1} geotherm at Atla Regio.

Comparison of the deformation styles and geodynamically inferred heat flows of features on Venus provides insight on the thermal evolution of the planet. Coronae and volcanoes may exhibit higher heat flows because the lithosphere in which they formed was younger at the time of loading than the lithosphere at Artemis, and/or these structures were responsible for thermal rejuvenation of the lithosphere. Coronae are inferred to be relatively older than large volcanoes; both feature types are about one-fourth to one-half the mean surface age on average [Price and Suppe, 1994; Namiki and Solomon, 1994]. The unique style of the Artemis underthrusting compared to other, older contractional structures on the planet [Brown and Grimm, 1995] and the possible age–heat flux correlation suggested here are concordant signs that, on average, the venusian lithosphere has monotonically cooled in the last several hundred million years [Turcotte, 1993; Arkani-Hamed *et al.*, 1993].

If we pose the surface temperature gradient as a function of age (t) for a semi-infinite half-space cooling model, we obtain [Turcotte and Schubert, 1982, pp. 158–167]

$$\frac{dT}{dz} = \frac{T_m - T_s}{\sqrt{\pi \kappa t}} \quad (11)$$

where T_m is the zero-age, or mantle, temperature. If the age of the lithosphere at the time of loading was 400 Ma (the mean surface age), (11) predicts $dT/dz = 5.1 \text{ K km}^{-1}$ for a nominal T_m of 1750 K . Because local geotherms below 4 K km^{-1} are inferred even for the strong rheology (Table 3), we must modify our assumptions.

We consider three end-member options. (1) The last global resurfacing event completely reassimilated the preexisting lithosphere, after which the present lithosphere began to form; thus, t should correspond to the age of this event. We would then infer that $t > 400 \text{ Ma}$ to satisfy the lowest geotherm. The upper bound on the surface age derived from crater statistics is $\sim 800 \text{ Ma}$ [Phillips *et al.*, 1992], for which we calculate $dT/dz = 3.6 \text{ K km}^{-1}$. (2) The resurfacing event may have reduced, but not completely reset, the lithospheric thermal age. For example, limited extensional processes could have induced sufficient magmatism without forming entirely new lithosphere [Grimm and Hess, 1996]. In this case, the observed surface age only furnishes a lower limit on the effective thermal age. (3) The mantle may have become abnormally cool by the time the lithosphere began to form [Arkani-Hamed *et al.*, 1993]. To achieve a 4 K km^{-1} geotherm at 400 Ma , we would require $T_m = 1550 \text{ K}$. In summary, any of these three, simple, end-member scenarios taken alone can explain a 4 K km^{-1} temperature gradient in the context of the half-space cooling model. Our flexural results admit, but do not require, lower heat flows; some combination of the above schemes would be required if the geotherm was as low as 3 K km^{-1} .

Conclusions

This study of flexure at Artemis Chasma provides insights into the fallibility of elastic flexure models, the rheology of the lithosphere, the forces responsible for Artemis, and the recent thermal state of Venus.

1. The elastic plate bending model, coupled with the moment–curvature matching technique, is generally not accurate when an in-plane force is present. Because in-plane stresses might play an important role in tectonics and flexure both elsewhere on Venus and in subduction settings on Earth, their omission from flexure models may introduce significant errors into estimates of lithospheric thermal structure [Mueller and Phillips, 1995]. A simple, though incomplete, test of the validity of the moment–curvature matching technique is to compare an inelastic synthetic flexural profile (generated at the geotherm inferred via the elastic fit) to the observed topography (Figure 5). The agreement between the temperature gradients found from the elastic and fully inelastic models is attributed to the range of in-plane force–geotherm combinations capable of reproducing a given flexural profile. If the in-plane force was somehow independently known, the “true” inelastic geotherm could be quite different from the one derived from the moment–curvature matching technique.

2. For a lithospheric rheology based on standard extrapolations of rock mechanics experiments, the inelastic flexure model indicates that thermal gradients for at least some parts of southeast Artemis must be less than 3.4 K km^{-1} (Table 3). Applying the strongest rheology we judge plausible, the geotherm must be less than 4 K km^{-1} for the widest outer rise cross sections. Narrower portions of the outer rise could be consistent with either higher geotherms ($< 6.4 \text{ K km}^{-1}$) or locally weaker lithosphere.

3. The flexural bending moment is of the order of $-7 \times 10^{17} \text{ N}$. Bending moments are not directly convertible from the slab density anomaly, which is also compensated by other mechanisms. The negatively buoyant underthrust slab at Artemis is the primary source of the flexural moment.

4. A sizable, compressive in-plane force of the order of $-1 \times 10^{14} \text{ N m}^{-1}$ is required by both the flexural modeling and the lack of outer trench slope faulting; it is also expressed by the pervasive wrinkle ridges on the southeast plains. Mantle flow coupling and lithospheric thinning might supply adequate driving forces. Surface faulting on the outer trench wall is precluded only if the in-plane force increases across this zone and if near-surface strength is at least a few tens of megapascals.

5. As a zone of underthrusting, Artemis should enforce upper bounds on heat flow at the time of loading. The low temperature gradients—comparable to those of the Moon—attest to the exceptional cooling that has occurred in the last few hundred million years of venusian thermal evolution. Our results favor a thick ($> 300\text{-km}$) thermal lithosphere [Kucinskis and Turcotte, 1994]. The low heat flux complies with the half-space cooling model if the thermal age of the lithosphere is over 600 Ma and/or the mantle temperature is as low as 1550 K .

6. The uniform, “plate-like” motions observed at Artemis Chasma reflect a spatially coherent tectonic style that is unusual on Venus [Brown and Grimm, 1995]. Deformation involves throughgoing failure and modest translation ($< 250 \text{ km}$) of a rigid lithosphere, distinct from the distributed, crust-dominated tectonics seen elsewhere on the planet. The thermal

maturity of the lithosphere documented in this study corroborates the strong-lithosphere behavior inferred from the tectonics of Artemis.

Acknowledgments. We are grateful to Steve Mueller for sharing his codes for the solution of the inelastic flexure equation. Catherine Johnson and Roger Phillips provided constructive reviews. This work was partially funded by NASA under the Venus Data Analysis Program, grant NAGW-3544. C.D.B. also received support from a NASA Space Grant Fellowship.

References

- Arkani-Hamed, J., G. G. Schaber, and R. G. Strom, Constraints on the thermal evolution of Venus inferred from Magellan data, *J. Geophys. Res.*, **98**, 5309–5315, 1993.
- Bai, Q., S. J. Mackwell, and D. L. Kohlstedt, High-temperature creep of olivine single crystals, I, Mechanical results for buffered samples, *J. Geophys. Res.*, **96**, 2441–2463, 1991.
- Brace, W. F., and D. L. Kohlstedt, Limits on lithospheric stress imposed by laboratory experiments, *J. Geophys. Res.*, **85**, 6248–6252, 1980.
- Brown, C. D., and R. E. Grimm, Tectonics of Artemis Chasma: A venusian "plate" boundary, *Icarus*, **117**, 219–249, 1995.
- Byerlee, J., Friction of rocks, *Pure Appl. Geophys.*, **116**, 615–626, 1978.
- Chopra, P. N., and M. S. Paterson, The role of water in the deformation of dunite, *J. Geophys. Res.*, **89**, 7861–7876, 1984.
- Dahlen, F. A., Isostasy and the ambient state of stress in the oceanic lithosphere, *J. Geophys. Res.*, **86**, 7801–7807, 1981.
- Davies, G. F., Mechanics of subducted lithosphere, *J. Geophys. Res.*, **85**, 6304–6318, 1980.
- Davies, G. F., Regional compensation of subducted lithosphere: Effects on geoid, gravity, and topography from a preliminary model, *Earth Planet. Sci. Lett.*, **54**, 431–441, 1981.
- Evans, B., and C. Goetze, The temperature variation of hardness of olivine and its implication for polycrystalline yield stress, *J. Geophys. Res.*, **84**, 5505–5524, 1979.
- Ford, P. G., and G. H. Pettengill, Venus topography and kilometer-scale slopes, *J. Geophys. Res.*, **97**, 13,103–13,114, 1992.
- Fung, Y. C., *Foundations of Solid Mechanics*, 525 pp., Prentice-Hall, Englewood Cliffs, N. J., 1965.
- Goetze, C., The mechanisms of creep in olivine, *Philos. Trans. R. Soc. London A*, **288**, 99–119, 1978.
- Goetze, C., and B. Evans, Stress and temperature in the bending lithosphere as constrained by experimental rock mechanics, *Geophys. J. R. Astron. Soc.*, **59**, 463–478, 1979.
- Goodman, R. E., *Introduction to Rock Mechanics*, 562 pp., John Wiley, New York, 1989.
- Grimm, R. E., The deep structure of venusian plateau highlands, *Icarus*, **112**, 89–103, 1994.
- Grimm, R. E., and P. C. Hess, The crust of Venus, in *Venus II*, edited by S. W. Bougher, D. M. Hunten, and R. J. Phillips, in press, Univ. of Ariz., Tucson, 1996.
- Jaeger, J. C., and N. G. W. Cook, *Fundamentals of Rock Mechanics*, 513 pp., Methuen, New York, 1969.
- Jarrard, R. D., Relations among subduction parameters, *Rev. Geophys.*, **24**, 217–284, 1986.
- Johnson, C. L., and D. T. Sandwell, Lithospheric flexure on Venus, *Geophys. J. Int.*, **119**, 627–647, 1994.
- Jones, G. M., T. W. C. Hilde, G. F. Sharman, and D. C. Agnew, Fault patterns in outer trench walls and their tectonic significance, in *Geodynamics of the Western Pacific*, edited by S. Uyeda, R. W. Murphy, and K. Kobayashi, pp. 85–101, Jpn. Sci. Soc., Tokyo, 1979.
- Karato, S., M. S. Paterson, and J. D. FitzGerald, Rheology of synthetic olivine aggregates: Influence of grain size and water, *J. Geophys. Res.*, **91**, 8151–8176, 1986.
- Kirby, S. H., Rheology of the lithosphere, *Rev. Geophys. Space Phys.*, **21**, 1458–1487, 1983.
- Kohlstedt, D. L., B. Evans, and S. J. Mackwell, Strength of the lithosphere: Constraints imposed by laboratory experiments, *J. Geophys. Res.*, **100**, 17,587–17,602, 1995.
- Kucinskias, A. B., and D. L. Turcotte, Isostatic compensation of equatorial highlands on Venus, *Icarus*, **112**, 104–116, 1994.
- Levitt, D. A., and D. T. Sandwell, Lithospheric bending at subduction zones based on depth soundings and satellite gravity, *J. Geophys. Res.*, **100**, 379–400, 1995.
- Liu, H. P., The structure of the Kurile Trench–Hokkaido Rise system computed by an elastic time-dependent plastic plate model incorporating rock deformation data, *J. Geophys. Res.*, **85**, 901–912, 1980.
- Mackwell, S. J., M. E. Zimmerman, D. L. Kohlstedt, and D. S. Scherber, Experimental deformation of dry Columbia diabase: Implications for tectonics on Venus, in *Rock Mechanics: Proceedings of the 35th U.S. Symposium*, edited by J. J. K. Daeman and R. A. Schultz, pp. 207–214, Balkema, Rotterdam, 1995.
- McAdoo, D. C., J. G. Caldwell, and D. L. Turcotte, On the elastic-perfectly plastic bending of the lithosphere under generalized loading with application to the Kuril Trench, *Geophys. J. R. Astron. Soc.*, **54**, 11–26, 1978.
- McGovern, P. J., M. Simons, and S. C. Solomon, Estimates of elastic lithosphere thickness and heat flux beneath large volcanoes on Venus (abstract), *Lunar Planet. Sci.*, **26**, 941–942, 1995.
- McKenzie, D. P., Speculations on the consequences and causes of plate motions, *Geophys. J. R. Astron. Soc.*, **18**, 1–32, 1969.
- McNutt, M. K., Lithospheric flexure and thermal anomalies, *J. Geophys. Res.*, **89**, 11,180–11,194, 1984.
- McNutt, M. K., and H. W. Menard, Constraints on yield strength in the oceanic lithosphere derived from observations of flexure, *Geophys. J. R. Astron. Soc.*, **71**, 363–394, 1982.
- McQueen, H. W. S., and K. Lambeck, The accuracy of some lithospheric bending parameters, *Geophys. J.*, **96**, 401–413, 1989.
- Mueller, S., and R. J. Phillips, On the reliability of lithospheric constraints derived from models of outer-rise flexure, *Geophys. J. Int.*, **123**, 887–902, 1995.
- Mueller, S., G. L. Choy, and W. Spence, Inelastic models of lithospheric stress, I, Theory and application to outer-rise plate deformation, *Geophys. J. Int.*, **125**, 39–53, 1996.
- Myers, J., and H. P. Eugster, The system Fe-Si-O: Oxygen buffer calibrations to 1500 K, *Contrib. Mineral. Petrol.*, **82**, 75–90, 1983.
- Namiki, N., and S. C. Solomon, Impact crater densities on volcanoes and coronae on Venus: Implications for volcanic resurfacing, *Science*, **265**, 929–933, 1994.
- Parmentier, E. M., and P. C. Hess, Chemical differentiation of a convecting planetary interior: Consequences for a one plate planet such as Venus, *Geophys. Res. Lett.*, **19**, 2015–2018, 1992.
- Parsons, B., and P. Molnar, The origin of outer topographic rises associated with trenches, *Geophys. J. R. Astron. Soc.*, **45**, 707–712, 1976.
- Paterson, M. S., *Experimental Rock Deformation—The BrITTLE Field*, 254 pp., Springer-Verlag, New York, 1978.
- Phillips, R. J., A mechanism for tectonic deformation on Venus, *Geophys. Res. Lett.*, **13**, 1141–1144, 1986.
- Phillips, R. J., Convection-driven tectonics on Venus, *J. Geophys. Res.*, **95**, 1301–1316, 1990.
- Phillips, R. J., Estimating lithospheric properties at Atla Regio, Venus, *Icarus*, **112**, 147–170, 1994.
- Phillips, R. J., R. F. Raubertas, R. E. Arvidson, I. C. Sarkar, R. R. Herrick, N. Izenberg, and R. E. Grimm, Impact craters and Venus resurfacing history, *J. Geophys. Res.*, **97**, 15,923–15,948, 1992.
- Phillips, R. J., C. L. Johnson, S. J. Mackwell, P. Morgan, D. T. Sandwell, and M. T. Zuber, Lithospheric mechanics and dynamics of Venus, in *Venus II*, edited by S. W. Bougher, D. M. Hunten, and R. J. Phillips, in press, Univ. of Ariz., Tucson, 1996.
- Press, W. H., S. A. Teukolsky, W. T. Vetterling, and B. P. Flannery, *Numerical Recipes in C*, 994 pp., Cambridge Univ. Press, New York, 1992.
- Price, M., and J. Suppe, Mean age of rifting and volcanism on Venus deduced from impact crater densities, *Nature*, **372**, 756–759, 1994.
- Sandwell, D. T., and G. Schubert, Flexural ridges, trenches, and outer rises around coronae on Venus, *J. Geophys. Res.*, **97**, 16,069–16,083, 1992a.
- Sandwell, D. T., and G. Schubert, Evidence for retrograde lithospheric subduction on Venus, *Science*, **257**, 766–770, 1992b.
- Schaber, G. G., R. G. Strom, H. J. Moore, L. A. Soderblom, R. L. Kirk, D. J. Chadwick, D. D. Dawson, L. R. Gaddis, J. M. Boyce, and J. Russell, Geology and distribution of impact craters on Venus: What are they telling us?, *J. Geophys. Res.*, **97**, 13,257–13,301, 1992.
- Schubert, G., W. B. Moore, and D. T. Sandwell, Gravity over coronae and chasmata on Venus, *Icarus*, **112**, 130–146, 1994.
- Schultz, R. A., Brittle strength of basaltic rock masses with applications to Venus, *J. Geophys. Res.*, **98**, 10,883–10,895, 1993.
- Shimada, M., A. Cho, and H. Yukutake, Fracture strength of dry silicate rocks at high confining pressures and activity of acoustic emission, *Tectonophysics*, **96**, 159–172, 1983.

- Sibson, R. H., A note on fault reactivation, *J. Struct. Geol.*, 7, 751–754, 1985.
- Sjogren, W. L., J. Arkani-Hamed, G. Balmino, W. B. Banerdt, J. P. Barriot, P. W. Chodas, T. R. Colvin, M. E. Davies, and A. S. Konopliv, Venus gravity field and other geodetic parameters, in *Venus II*, edited by S. W. Bougher, D. M. Hunten, and R. J. Phillips, in press, Univ. of Ariz., Tucson, 1996.
- Spence, W., Slab pull and the seismotectonics of subducting lithosphere, *Rev. Geophys.*, 25, 55–69, 1987.
- Tsenn, M. C., and N. L. Carter, Upper limits of power law creep of rocks, *Tectonophysics*, 136, 1–26, 1987.
- Turcotte, D. L., An episodic hypothesis for venusian tectonics, *J. Geophys. Res.*, 98, 17,061–17,068, 1993.
- Turcotte, D. L., and G. Schubert, *Geodynamics*, 450 pp., John Wiley, New York, 1982.
-
- C. D. Brown and R. E. Grimm, Department of Geology, Arizona State University, Box 871404, Tempe, AZ 85287-1404. (e-mail: dbrown@violetta.la.asu.edu; bob.grimm@asu.edu)

(Received November 9, 1995; revised March 1, 1996; accepted March 12, 1996.)